Journal of Ceramic Processing Research. Vol. 15, No. 2, pp. 82~87 (2014)

J O U R N A L O F
Ceramic Processing Research

Rapid low-temperature consolidation of nanocrystalline Co-ZrO_2 composite by high frequency induction heating and its mechanical properties

In-Jin Shon* and Na-Ra Park

Division of Advanced Materials Engineering, the Research Center of Advanced Materials Development, Chonbuk National University, 664-14 Deokjin-dong 1-ga, Deokjin-gu, Jeonju, Jeonbuk 561-756, Korea

Prior to sintering, two kinds of powders were produced by milling Co_3O_4 and Zr as raw powder with each other's milling method such as horizontal ball milling and high energy ball milling. The first one was mixed as Co_3O_4 and Zr powders during horizontal ball milling and the other milled powder was synthesized as Co and ZrO_2 powders during high energy ball milling. Each of the milled powders was consolidated by the High Frequency Induction Heated Sintering method within 3 minutes under the 1 GPa pressure, respectively. The relative densities of these specimens sintered from HFIHS were measured by the Archimedes method. The crystallite sizes of Co and ZrO_2 in each composite were calculated by Suryanarayana and Grant Norton's formula. The mechanical properties of Co-ZrO_2 composites consolidated by HFIHS from the horizontal ball milling method and high energy ball milling method were investigated from each surface indentation.

Key words: Co-ZrO_2, Composite, Sintering, Mechanical properties, Nanocrystalline.

Introduction

Metal matrix composite has received much attention for the performance requirement of materials regarding aerospace and automotive applications. In order to be utilized in these fields, MMC materials need to require the following characteristics such as high strength, high fracture toughness, good wear resistance, good oxygen resistivity, good corrosion resistance, good chemical stability and so on. Therefore, since it has a significant role in improving the above characteristics thanks to interfacial reactivity, wet ability, microstructural stability and microstructural homogeneity, we used the in-situ process even though the in-situ method can lead to create unexpected products which might be a tiny portion in Co-ZrO_2 composites.

One of the main purposes of this study regards the use for prosthetic joint replacement. As we are living in an aging society these days, the need of prosthetic joint replacement is going to be higher than ever. Ceramics have been used as an alternative to metal-on-polyethylene in joint replacement surgery of arthritic hips and knees since the 1970s. However, ceramics are so brittle that in vivo failure can result from the fracture of the ceramic femoral head and fracture of the ceramic acetabular liner [1] because of the low toughness of ceramics. Therefore, we produced the Co-ZrO_2 composite in order to improve toughness.

*Corresponding author:
Tel : +82-63-270-2381
Fax: +82-63-270-2386
E-mail: ijshon@chonbuk.ac.kr

It is one of main keys to control grain growth during sintering from nanosized powder. The grain size in sintered materials becomes much larger than that in pre-sintered powders due to a fast grain growth during the conventional sintering process. In this regard, the high frequency induction heated sintering method which can make dense materials within 3 minutes has been shown to be effective in achieving this goal [2-4]. The HFIHS also takes an advantage of applying mechanical pressure and induced current during sintering, simultaneously. As a result, the sintering temperature is expected to decrease because applying mechanical pressure affects the driving force of the sintering.

Experimental Procedure

Fig.1 shows the Co_3O_4 powder having an angular shape and the Zr powder having an irregular shape. The powders of 99.5% Co_3O_4 (< 10 μm, Aldrich, Inc) and 99.5% pure Zr(−325 mesh, Sejong, Inc) as raw materials were prepared in order to be mixed and synthesized. First of all, the horizontal ball milling method was conducted with ethanol in a polyethylene bottle for 10 h and the horizontal rotational velocity was 250 rpm. The ratio for the weight of ball-to-powder was 10 : 1. Secondly, the raw materials were milled at 250 rpm for 10 h by the high energy ball milling method that was able to be synthesized. Tungsten carbide balls (8.5 mm in diameter) were used in a sealed cylindrical stainless steel vial under an argon atmosphere. The weight ratio of ball-to-powder was 30 : 1. The grain sizes of the mixed Co_3O_4 and Zr powders were calculated by Suryanarayana and

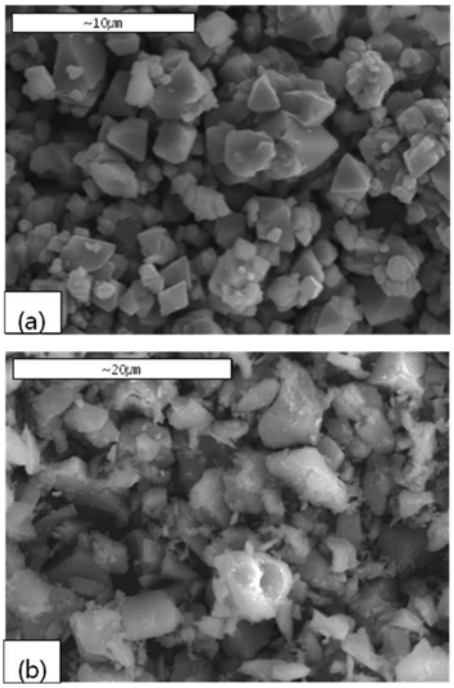

Fig. 1. Scanning electron microscope image of raw materials: (a) Co_3O_4, (b) Zr.

Grant Norton's formula and those of the mechanical synthesized powders were the same. Suryanarayana and Grant Norton's formula is [5]:

$$B_r(B_{crystalline}+B_{strain})cos\,\theta = k\lambda/L + \eta sin\,\theta \quad (1)$$

where B_r is the full width at half-maximum (FWHM) of the diffraction peak after instrumental correction; $B_{crystalline}$ and B_{strain} are FWHM caused by small grain size and internal stress, respectively; k is constant (with a value of 0.9); λ is wavelength of the X-ray radiation; L and η are grain size and internal strain, respectively; and θ is the Bragg angle. The parameters B and B_r follow Cauchy's form with the relationship: $B = B_r + B_s$, where B and B_s are FWHM of the broadened Bragg peaks and the standard sample's Bragg peaks, respectively.

After milling, the mixed and the alloyed powders were placed in a WC die (outside diameter, 40 mm; inside diameter, 5 mm; height, 40 mm) and then the induced current was introduced into the WC die. The HFIHS system made by Eltek in South Korea was shown schematically in Fig. 2. The four major stages in the sintering process are as follows. Stage 1 involves making the system create a vacuum. Stage 2 applies a uniaxial pressure of 1 GPa. Stage 3 requires flowing an induced current into the system and maintains it at 600 ºC with a heating rate of 200 ºC/min and then the system is turned off without a holding time. A pyrometer focused on the surface of the WC die is used for measuring the temperature during HFIHS. Lastly, stage 4 is to cool the sample to room temperature. The process was carried out under a vacuum of 5.33 Pa.

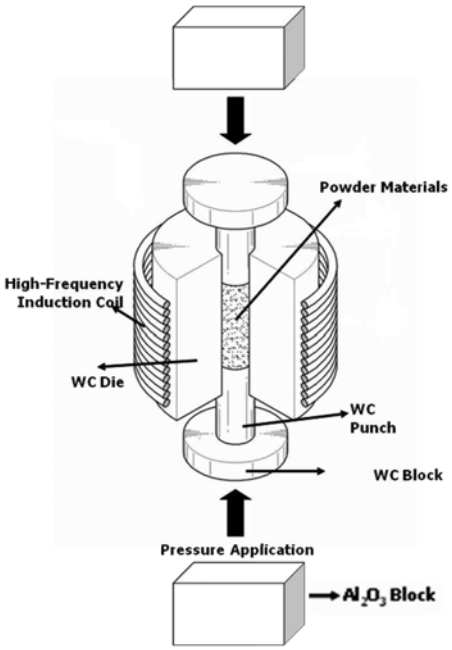

Fig. 2. Schematic diagram of the high frequency induction heated sintering apparatus.

The relative densities of the sintered samples were measured by the Archimedes method. Compositional and micro structural analyses of the products which were policed were made through X-ray diffraction (XRD) and scanning electron microscopy (SEM) with energy dispersive X-ray analysis (EDAX). Vickers hardness was measured by performing indentations at a load of 10 kg and a dwell time of 15 s on the sintered samples.

Lastly, the cytotoxicity test was conducted by using the fibroblast cell. The fibroblasts were proliferated in

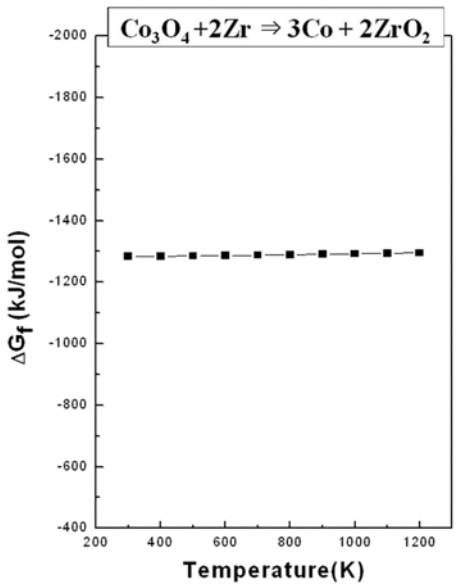

Fig. 3. Temperature dependence of the Gibbs free energy variation by interaction of Co_3O_4 with 2 Zr.

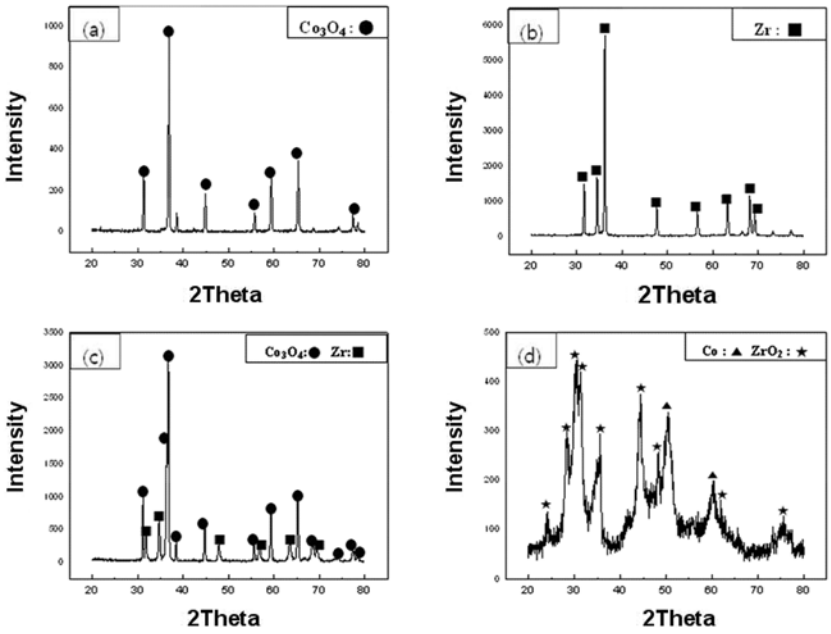

Fig. 4. XRD patterns of raw materials: (a) Co_3O_4, (b) Zr, (c) horizontal milled powders and (d) mechanically milled powders.

Dulbecco's Modified Eagle's Medium (DMEM) with 10% fetal bovine serum (FBS) at 37 ± 1 °C and then the concentration of the CO_2 was 5 ± 0.5%. After enough growth, the fibroblasts were seeded at a density of 7×10^3 cells per well into 96well cell culture plates. They were respectively cultured for 1, 3, and 7 days with 100 μl of media ionized from the Co-ZrO_2 composite. The cells were treated by using CCK-8 solution for 24 h. Absorbance was measured at 570 nm by using a microplate reader.

Results and Discussion

The interaction between Co_3O_4 and 2 Zr, i.e.,

$$Co_3O_4 + 2Zr \rightarrow 3Co + 2ZrO_2 \quad (2)$$

is thermodynamically feasible as shown in Fig. 3.

The Fig. 4 indicates the x-ray diffraction pattern of raw materials, horizontal ball milled powder and high energy ball milled powder. In the XRD pattern results of Fig. 4(c) and (d), although the reactants were of the same materials, the products were different, which is because the high energy ball milling method generated higher energies than those of the horizontal ball milling during the milling process. From the above results, solid replacement reaction completely occurs during the high energy ball milling. The full width at half-maximum (FWHM) of the diffraction peak is broad due to the refinement of powder and increase of strain. The average grain sizes of ZrO_2 measured by Suryanarayana and Grant Norton's formula were approximately 16 nm.

After milling, each milled powder was consolidated by HFIHS at 600 °C within 3min. These powders were sintered at a much lower temperature by applying high-pressure. (1 GPa) which have a significant effect on the surface energy driving force such that the total driving force, F_D, is now [6]

$$F_D = \gamma + (P_a r/\pi), \quad (3)$$

where γ is the surface energy, Pa is the applied pressure, and r is the radius of the particle. The effect of pressure on the densification of TiO_2 during high-frequency induction heated sintering was investigated by Shon *et al*. [7]. A significant increase in the relative density was observed as the pressure was increased from about 60 to 100 MPa for sintering at 800 °C. Secondly, the role of the current (resistive or inductive) in sintering and or synthesis has been the focus of several attempts aimed at providing an explanation to the observed enhancement of sintering and the improved characteristics of the products. The role played by the current has been variously interpreted, the effect being explained in terms of the fast heating rate due to Joule heating, the presence of plasma in pores separating powder particles, and the intrinsic contribution of the current to mass transport [8-11].

Fig. 5 represents XRD patterns of the specimens sintered by HFIHS from high energy ball milled powder (a) and horizontal ball milled powder (b). We assumed that the powders mixed by the horizontal ball milling method were simultaneously synthesized and consolidated during the sintering process since the peaks of Co and ZrO_2 were detected from XRD data. Fig. 6 indicates the plot of $B_r\cos\theta$ versus $\sin\theta$ of ZrO_2 in the composites sintered from (a) horizontal ball milled powders and (b) high energy ball milled powders.

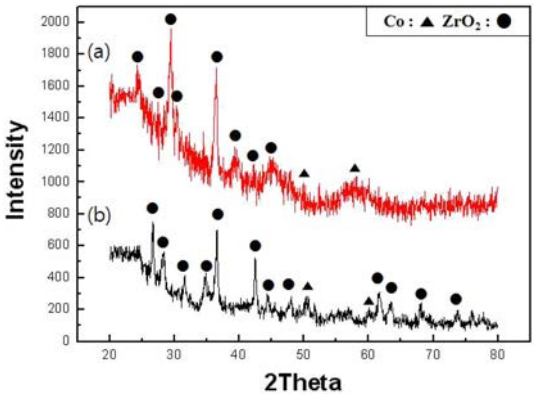

Fig. 5. XRD patterns of Co-ZrO_2 composite sintered from (a) high energy ball milled powders and (b) horizontal milled powders.

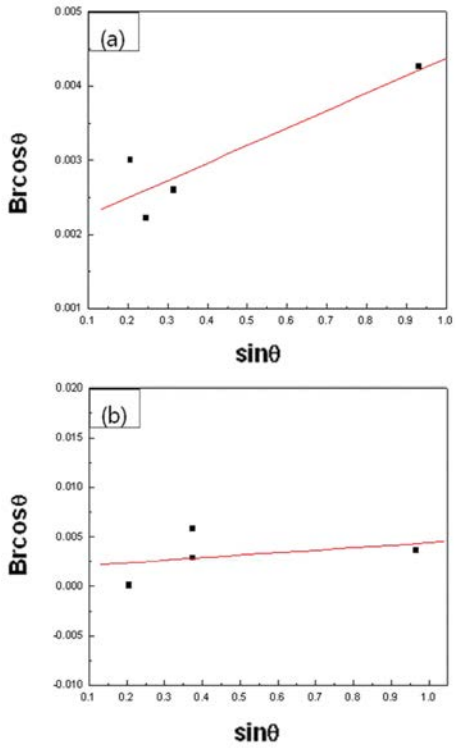

Fig. 6. Plot of $B_r\cos\theta$ versus $\sin\theta$ of ZrO_2 in composite sintered from (a) horizontal milled powders and (b) high energy ball milled powders.

The grain sizes of ZrO_2 in each of the composites calculated by Suryanarayana and Grant Norton's formula was 170 and 73 nm, respectively. The reason that the grain size of ZrO_2 milled by the horizontal ball milling method is far higher than those milled by the high energy ball milling method is combustion synthesis. The microstructure of the Co-ZrO_2 composite sintered from high energy ball milled powder was shown in Fig. 7. In this FE-SEM image, we can realize that nanocrystalline ZrO_2 was well dispersed in the Co-ZrO_2 composite. The atomic structure of Co-ZrO_2 composite could be found in Fig. 8. The TEM image revealed that microstructures were well bonded. Each of the grain boundaries was divided from an atomic

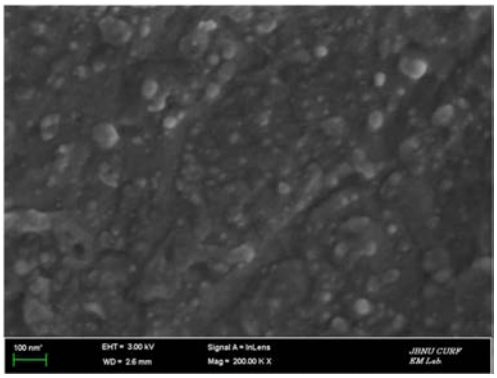

Fig. 7. FE-SEM images of Co-ZrO_2 composite sintered from high energy ball milled powders.

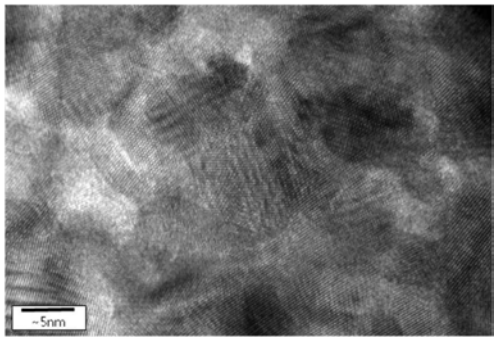

Fig. 8. TEM image of Co + ZrO_2 sintered from high energy ball milled powders.

structure and we can also see that grains are nano-sized.

Vickers hardness indentations were made on polished sections of the Co-ZrO_2 composite using a 10 kg_f load for a 15s dwell time. The calculated hardness values of Co-ZrO_2 composites sintered at 600 ºC from horizontal milled powders and high energy ball milled powders were 3.6 and 4.3 GPa, respectively. These values represent the averages of five measurements. Indentations with large enough loads produced median cracks around the indentations. The length of these cracks permits an estimation of the fracture toughness for the material. From the length of these cracks, fracture toughness values can be determined using the formula by Anstis *et al*. [12] is

$$K_{IC} = 0.016\ (E/H)^{1/2} \cdot P/C^{3/2} \quad (4)$$

where E is Young's modulus, H the indentation hardness, P the indentation load, and C the trace length of the crack measured from the center of the indentation. The modulus was estimated by the rule of mixtures for the 0.69 volume fraction of ZrO_2 and the 0.31 volume fraction of Co using $E(ZrO_2) = 207$ GPa [8] and $E(Co) = 209$ Gpa [13]. As in the case of hardness values, the toughness values were derived from the average of five measurements. Furthermore, the toughness values of composites obtained from

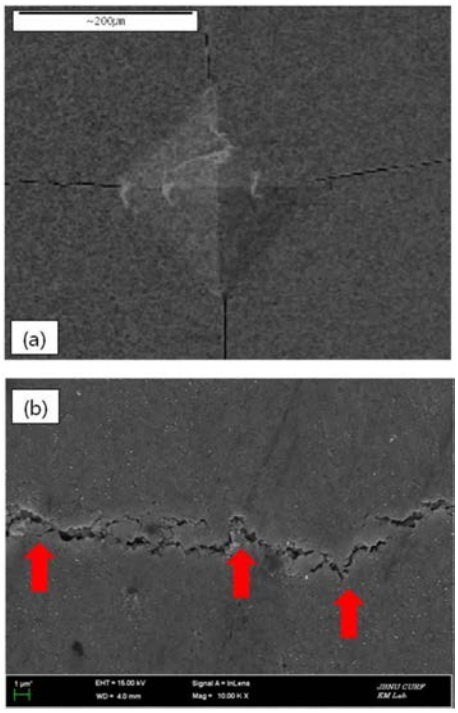

Fig. 9. (a) Vickers hardness indentation and (b) median crack propagated in the Co-ZrO_2 composite sintered from high energy ball milled powders.

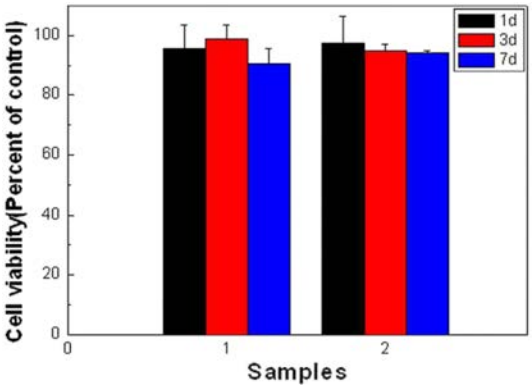

Fig. 10. Measurement of cellular viability in Ti(1) and Co + ZrO_2(2) composite by CCK-8 assay on 1, 3, and 7days.

horizontal milled powders and high energy ball milled are 9.8, 10.2 MPa · $m^{1/2}$, respectively.

The hardness and fracture toughness of ZrO_2 are reported as 11.8 GPa and 6.5 MPa · $m^{1/2}$, respectively [14]. The hardness of the 3Co-2ZrO_2 composite is lower than that of monolithic ZrO_2 but the fracture toughness is higher than that of ZrO_2 due to the addition of ductile Co. Fig. 9 (a) displays Vickers indentation in the 3Co-2ZrO_2 composite sintered from high energy ball milled powders. One to three additional cracks were observed to propagate from the indentation corner. We also thought that crack propagated accordig to the grain boundary of Co, but the crack was diffracted by running into nano-sized ZrO_2 (↑) in Fig. 9(b).

Fig. 10 shows the cytotoxicity test of Co-ZrO_2 composite, which is measured by the CCK-8 assay. The CCK-8 assay is one of the most convenient methods using highly water-soluble tetrazolium salt. By adding tetrazolium to media, we can quantify cell viability as tetrazolium would change specific color reacted by the dehydrogenase of mitochondria. The value of the cell viability regarding the Co-ZrO_2 composite was of similar value compared to Ti, which is widely known to be used for in-vivo materials.

Conclusions

The mixed powders and mechanical synthesized powder were fabricated by each other's milling method. These milled powders were densified by HFIHS within 3 min and the relative densities of the sintered specimens were 92% and 97%, respectively. Although the components of both specimens were Co and ZrO_2 through XRD data, the average grain size of the ZrO_2 in composites sintered from mechanically synthesized powders was 73 nm and this size was much lower than that from horizontal ball milled powders. The average hardness and fracture toughness values obtained from mechanically synthesized powders and horizontal milled powders were 4.3, 3.6 GPa and 10.2, 9.8 MPa · $m^{1/2}$, respectively. Lastly, the cell viability portion was higher than 90%, which means that the Co-ZrO_2 composite exhibited zero toxicity.

Acknowledgments

This research was supported by Basic Science Research Program through the National Research Foundation of Korea (NRF) funded by the Ministry of Education (2012R1A1A4A01001300) and follows the results of a study of the "Leaders Industry-university Cooperation" Project, supported by the Ministry of Education, Science & Technology (MEST).

References

1. Mohamed N, Rahaman and Aihua Yao, Journal of the American Ceramic Society 90 [7] (2007) 1965-1988.
2. S.M. Kwak, H.K. Park, I.J. Shon, Korean J. Met. Mater. 51, (2013) 314-348.
3. G.W. Lee, I.J. Shon, Korean J. Met. Mater. 51, (2013) 95-100.
4. In-Jin Shon, Kwon-Il Na, Hyun-Kuk Park, Sung-Wook Cho, Jae-Won Lim, Wonbaek Kim, Journal of Ceramic Processing Research, 13 (2012) 441-445.
5. C.Suryanarayana, and M.Grant Norton, X-ray Diffraction A Practical Approach, Plenum Press, New York, (1998).
6. R. L. Coble, J. Appl. Phys. 41 (1970) 4798-4807.
7. Hwan-Cheol, Hyun-Kuk, In-Jin Shon, In-Yong Ko, Journal of Ceramic Processing Research 7 (2006) 327-331.
8. Z. Shen, M. Johnsson, Z. Zhao and M. Nygren, J. Am. Ceram. Soc. 85 (2002) 1921-1927.
9. J. E. Garay, U. Anselmi-Tamburini, Z. A. Munir, S. C. Glade and P. Asoka- Kumar, Appl. Phys. Lett. 85 (2004)

573-597.
10. J. R. Friedman, J. E. Garay. U. Intermetallics 12 (2004) 589-597.
11. J. E. Garay, J. E. Garay. U. Anselmi-Tamburini and Z. A. Munir, Acta Mater. 51 (2003) 4487-4495.
12. G.R. Anstis, P. Chantikul, B.R. Lawn, D.B. Marshall, J. Am. Ceram. Soc. 64 (1981) 533-538.
13. http://en.wikipedia.org/wiki/Elastic properties of the elements (data page).
14. S.G. Huang, K. Vanmeensel, O. Van der Biest, J. Vleugels, Journal of the European Ceramics Society 27 (2007) 3269-3275.